

Towards Reliable Fetal Ultrasound Interpretation with Multi-Agent Collaboration

Xiaotian Hu^{a,1}, Mingxuan Liu^{a,1}, Junwei Huang^{a,1}, Kasidit Anmahapong^a,
Yifei Chen^a, Yiming Huang^b, Xuguang Bai^a, Zihan Li^a, Hongjia Yang^a,
Yingqi Hao^a, Hong Xu^c, Yu Jiang^c, Tian Tian^c, Yi Liao^c, Haibo Qu^{c,*},
Qiyuan Tian^{a,*}

^a*Tsinghua University, Beijing, China*

^b*University of California San Diego, La Jolla, CA, USA*

^c*West China Second University Hospital, Sichuan University, Chengdu, China*

Abstract

Automated fetal ultrasound interpretation spans from low-level visual perception (e.g., plane recognition and anatomical segmentation) to high-level clinical understanding (e.g., biometric measurement and diagnostic reporting). Deep learning models developed under the “one-task, one-model” paradigm impede systematic integration of perceptual evidence across the multi-step clinical workflow. Meanwhile, multimodal large language models (MLLMs) demonstrate promising visual understanding, yet limited domain-specific grounding and hallucination tendencies fundamentally constrain their reliability in fetal ultrasound analysis. To bridge this gap, we propose FetUSAgents, the first tool-augmented multi-agent system for comprehensive fetal ultrasound interpretation, supporting visual question answering (VQA), report generation, image captioning, and video summarization. FetUSAgents orchestrates task-specific visual tools via collaborative LLM agents, decomposing complex clinical queries into manageable subtasks that advance from anatomical recognition to quantitative measurement, mirroring expert sonographers’ stepwise reasoning. Importantly, a Dual-Path Evidence Arbitration (DPEA) mechanism is proposed to integrate LLM-driven deliberative reasoning with

*Corresponding authors.

Email addresses: qiyuantian@tsinghua.edu.cn (Qiyuan Tian),
windowsqhb@126.com (Haibo Qu)

¹Xiaotian Hu, Mingxuan Liu, and Junwei Huang contributed equally to this work.

structured computational evidence from specialized visual tools. Concurrently, a retrieval-enhanced Evidence bank consolidates heterogeneous intermediate findings to promote traceable, clinically grounded conclusions. Furthermore, we introduce FetUS-VQA, the first dedicated VQA benchmark for fetal ultrasound, comprising 1,892 images and 3,205 question–answer pairs spanning 10 clinical tasks. Extensive out-of-distribution (OoD) experiments demonstrate that FetUSAgents consistently surpasses both general and medical MLLMs, exceeding the strongest baseline by over 25% in VQA accuracy, highlighting a scalable path toward evidence-driven clinical assistants for prenatal imaging. Code: <https://github.com/hu2274898/FetUSAgents>.

Keywords: LLM Agent, Fetal Ultrasound, Visual Question Answering, Report Generation

1. Introduction

Fetal ultrasound plays a central role in prenatal screening (Salomon et al., 2011) owing to its non-invasiveness, cost-effectiveness, and real-time imaging capability (He et al., 2021; Fiorentino et al., 2023a). In routine clinical practice, sonographers are required to identify standardized anatomical planes, delineate fine-grained fetal structures, and derive quantitative biometric measurements. However, these tasks must be performed within a dynamic scanning environment characterized by variable fetal positioning, acoustic shadowing, and limited soft-tissue contrast, rendering fetal ultrasound interpretation inherently subjective and highly operator-dependent (Maani et al., 2025). In resource-limited settings, the scarcity of experienced sonographers further exacerbates these challenges, restricting timely access to reliable prenatal assessment (Olagunju et al., 2025; Sippel et al., 2011). Consequently, there is a pressing need for AI-assisted solutions to enhance the objectivity, reproducibility, and accessibility of fetal ultrasound diagnosis.

Prior deep-learning approaches for fetal ultrasound predominantly follow a “one-task, one-model” paradigm. Task-specific models for plane classification, anatomical structure segmentation, and fetal biometry have demonstrated promising accuracy on in-distribution (ID) benchmarks (Zeng et al., 2022; Zhou et al., 2025). However, these models remain narrowly specialized and fragmented across workflows, typically deployed as standalone predictors that still require substantial manual coordination in clinical practice (Fiorentino et al., 2023b; Yan et al., 2025). Moreover, they are often developed on data

from specific centers, specific devices, and narrowly defined task settings, which limits their robustness and transferability across institutions, imaging devices, populations, and low-resource clinical environments(Fiorentino et al., 2023b).

Multimodal large language models (MLLMs)(Chen et al., 2024b; Sellergren et al., 2025), pretrained or fine-tuned on large-scale medical datasets spanning diverse imaging modalities, have emerged as a promising approach to addressing these limitations. By learning joint visual-textual representations, MLLMs have demonstrated encouraging performance in medical visual question answering (VQA) and report generation. Nevertheless, they remain constrained by opaque reasoning processes that lack traceable visual evidence and cannot readily incorporate external domain knowledge(Qi et al., 2026). Moreover, most MLLMs rely on monolithic end-to-end inference, limiting their ability to invoke specialized tools or coordinate multi-step clinical workflows(Chen et al., 2026). Their propensity for hallucination further poses substantial risks in safety-critical domains such as fetal ultrasound.

Tool-augmented agents alleviate the limited domain grounding, weak interpretability, and hallucination tendencies of end-to-end MLLMs by invoking external specialist tools and iteratively accumulating task-relevant evidence (Wang et al., 2026). Beyond tool use, LLM-driven agents introduce planning, memory, and role specialization, decomposing complex clinical queries into manageable subtasks while preserving intermediate evidence throughout the reasoning chain (Mao et al., 2026; Lyu et al., 2025). Collaborative multi-agent designs further enhance robustness through cross-verification and consultation-like deliberation, echoing multidisciplinary decision-making in clinical practice (Kim et al., 2024; Tang et al., 2024). Nevertheless, existing agentic systems target primarily radiology, pathology, and general medical imaging, leaving fetal ultrasound unexplored. Given its distinctive challenges of dynamic scanning, subtle anatomical variations, and measurement-oriented interpretation, a dedicated agent-based framework tailored to this domain is still lacking.

To bridge this gap, we propose FetUSAgents, the first tool-augmented multi-agent system specifically designed for fetal ultrasound interpretation. Given a user query and ultrasound input, FetUSAgents routes the request to the appropriate clinical workflow, identifies the anatomical context, and dispatches task-specific expert Agents to acquire structured visual evidence. A Dual-Path Evidence Arbitration (DPEA) mechanism then integrates deliberative reasoning from multiple LLM-based voters with computational

evidence from specialized tools, yielding decisions that are both clinically interpretable and data-grounded. A retrieval-enhanced Evidence bank further consolidates heterogeneous intermediate findings across the pipeline, strengthening factual grounding and reducing hallucination in the generated text. To systematically evaluate FetUSAgents, we constructed FetUS-VQA, the first comprehensive benchmark for fetal ultrasound, comprising 3,205 queries across 10 VQA subtasks derived from 7 clinical task categories (Fig. 2(a)). Extensive experiments on FetUS-VQA demonstrate that FetUSAgents consistently outperforms both general and medical MLLMs, exceeding the strongest competitor by over 25% in VQA accuracy.

The main contributions of this work are as follows:

1. We propose **FetUSAgents**, the first tool-augmented multi-agent system that enables general MLLMs to perform comprehensive fetal ultrasound interpretation, including VQA, report generation, and video summarization, without monolithic domain-specific retraining.
2. We introduce a Dual-Path Evidence Arbitration (DPEA) mechanism and a retrieval-enhanced Evidence bank to improve decision reliability and effectively reduce hallucination in clinical report generation.
3. We introduce FetUS-VQA, the first dedicated VQA benchmark for fetal ultrasound analysis. Extensive experiments on FetUS-VQA show that FetUSAgents consistently and significantly outperforms state-of-the-art (SOTA) general and medical MLLMs.

2. Related Work

2.1. Automatic Fetal Ultrasound Image Analysis

Deep-learning methods have been widely explored for fetal ultrasound analysis, spanning standard-plane classification, anatomical structure segmentation, and fetal biometry. Specifically, early CNN-based models such as SonoNet enabled real-time detection and weakly supervised localization of fetal standard planes (Baumgartner et al., 2017). Subsequent studies further advanced this task through systematic architecture evaluation (Burgos-Artizzu et al., 2020a), deep feature integration (Krishna and Kokil, 2023), and stacked ensemble learning (Krishna and Kokil, 2024). Additionally, anatomical segmentation benefited from U-Net variants augmented with attention mechanisms for fetal cerebellum delineation (Shu et al., 2022), lightweight multi-scale designs for four-chamber heart segmentation (Pu et al., 2022), and semi-supervised

strategies that alleviate pixel-level annotation demands(Pham et al., 2025). Quantitative biometry has likewise progressed from segmentation-based geometric fitting for Head Circumference (HC) and Abdominal Circumference (AC), and femur length (FL) estimation(Bano et al., 2021) toward landmark-based direct regression(Avisdris et al., 2022), whole-examination frame-wise aggregation(Venturini et al., 2025), and large-scale growth prediction beyond conventional Hadlock-style models(Mikołaj et al., 2025). More recently, foundation models such as FetalCLIP(Maani et al., 2025) and USFM(Jiao et al., 2024) have further advanced the field by enabling transferable representation learning across diverse downstream tasks. Despite these advances, most existing methods remain optimized for individual subtasks and lack the capacity to unify perceptual, quantitative, and interpretive stages into a coherent end-to-end clinical workflow.

2.2. Medical Agentic Systems

Medical agentic systems have emerged as a promising solution to the limitations of standalone MLLMs, demonstrating strong potential across clinical scenarios such as radiology(Mao et al., 2026; Wang et al., 2026; Qi et al., 2026), pathology(Lyu et al., 2025), and cardiology(Zhou et al., 2026). These systems typically coordinate multiple MLLM-based agents for debate, voting, or collaborative reasoning(Tang et al., 2024; Kim et al., 2024), or integrate specialized medical tools to support structured evidence acquisition and multistep clinical decision-making(Liu et al., 2026; Chen et al., 2026). However, to the best of our knowledge, existing agentic AI systems have not yet been specifically adapted to fetal ultrasound, whose ambiguous anatomical boundaries, limited soft-tissue contrast, operator-dependent image quality, and scarcity of annotated data impose particularly unique requirements on agent design.

3. Method

3.1. Overview

FetUSAgents (Fig. 1) is a tool-augmented multi-agent system built upon the AutoGen framework(Wu et al., 2024) for fetal ultrasound interpretation. Specifically, FetUSAgents comprises three core components: (1) a set of collaborative LLM-based agents that orchestrate task planning, deliberative reasoning, and report generation, unifying isolated visual predictors into a coherent clinical workflow (Sec. B); (2) a task-specific tool library of specialized

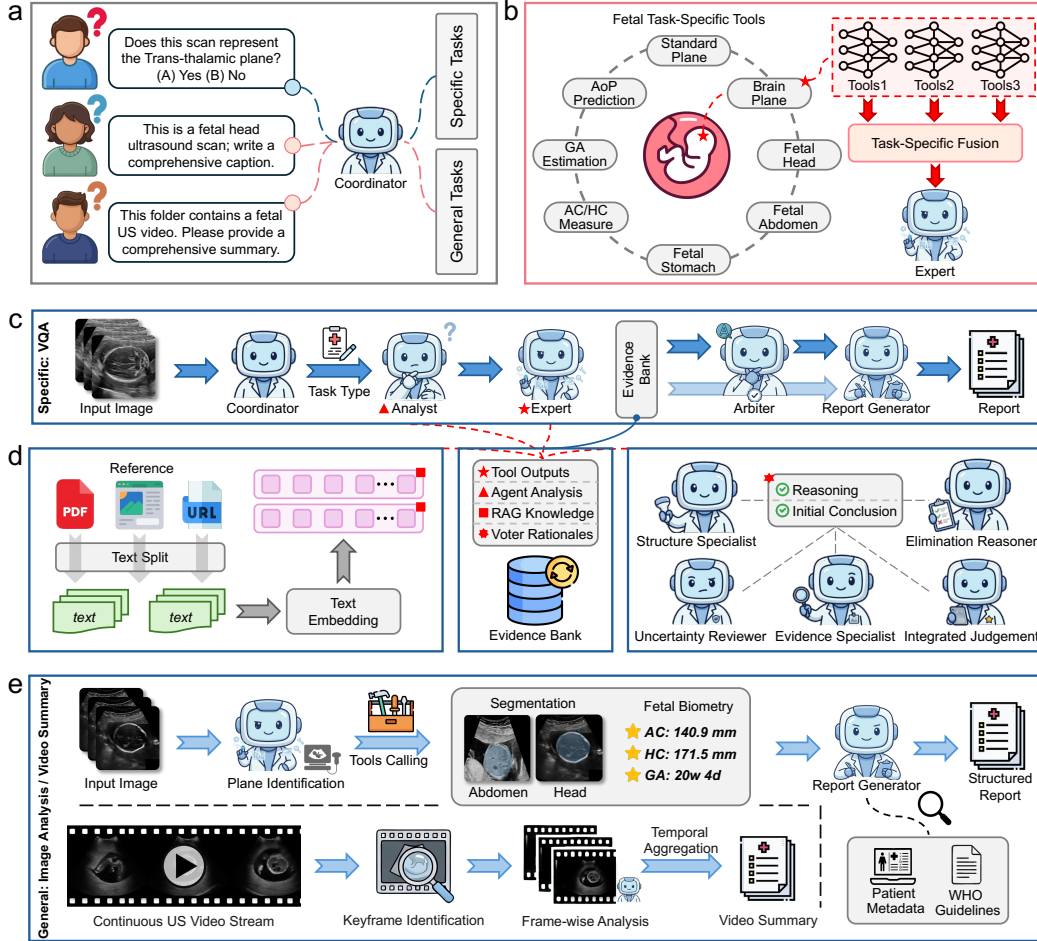


Figure 1: Overview of the FetUSAgents framework. The system routes user requests to specific-task or general-task workflows, invokes task-specific Expert Agents for visual evidence acquisition, integrates tool outputs with multi-agent deliberation through DPEA, and uses retrieval-enhanced evidence consolidation to support grounded report generation, image captioning, and video summarization.

visual tools that serve as independently callable services, providing trustworthy anatomical evidence for each clinical subtask (Sec. C); and (3) a DPEA mechanism (Sec. D) together with a retrieval-enhanced Evidence bank (Sec. E) that integrates computational tool evidence with LLM-driven deliberative reasoning and consolidates heterogeneous intermediate findings to reduce hallucination in report generation. Orchestrating these components, given multimodal inputs including a fetal US image I , a video sequence $V = \{I_t\}_{t=1}^T$,

and a user text query Q , FetUSAGents supports four clinical functions: VQA, report generation, image captioning, and video summarization.

3.2. Agent Roles

3.2.1. Coordinator Agent

The *Coordinator Agent* (Fig. 1(a)) serves as the central orchestrator of FetUSAGents, fulfilling two core responsibilities: (a) Query routing, which classifies user requests and dispatches them to the appropriate downstream workflow. Specifically, given a user query Q and an input image I or video V , the *Coordinator Agent* determines the query type $\tau \in \{\textit{specific}, \textit{general}\}$. Queries with an explicit question-and-option structure (e.g., VQA) are categorized as *specific*, whereas open-ended requests (e.g., image captioning and video summarization) are categorized as *general*. Accordingly, the Coordinator dispatches *specific* queries to the deliberative VQA pipeline (Sec. D) and *general* queries to the end-to-end clinical workflow (Sec. F). (b) Task allocation, which identifies the clinical task type t from inputs (i.e., Q, I), and activates the corresponding *Expert Agent* (Sec. B(3)) subset $E_{\text{selected}} \subseteq \{E_1, \dots, E_K\}$, which in turn invoke the relevant visual tools from the tool library (Sec. C).

3.2.2. Analyst Agent

The *Analyst Agent* parses the user query Q and input image I into a structured context representation A , which is shared with all downstream agents to support more focused reasoning.

3.2.3. Expert Agents

Each *Expert Agent* E_k is responsible for invoking a designated subset of visual tools $S_k = \{s_{k,1}, \dots, s_{k,N}\}$ from the task-specific tool library (Sec. C) and applying a task-appropriate fusion rule F_k (Sec. C) to aggregate their outputs into a unified prediction:

$$\hat{o}_k = F_k(s_{k,1}(I), \dots, s_{k,N}(I)), \quad (1)$$

where \hat{o}_k denotes the fused output of expert E_k .

3.2.4. Voter Agents

To incorporate complementary, image-grounded clinical reasoning from diverse diagnostic perspectives, five deliberative *Voter Agents* (Fig. 1(d), right) were included, denoted as $\mathcal{V} = \{V_j\}_{j=1}^5$. Given an input image I and a query Q , each voter V_j independently evaluates the case under a distinct

reasoning profile: (a) *Structure Specialist*, prioritizing anatomical identity recognition and key landmark localization; (b) *Evidence Specialist*, focusing on image appearance and morphological patterns; (c) *Elimination Reasoner*, adopting a differential-exclusion strategy that rules out implausible options first; (d) *Uncertainty Reviewer*, explicitly assessing evidence reliability and potential sources of ambiguity; and (e) *Integrated Judgement*, synthesizing all available cues into a globally coherent decision. This role diversification across the *Voter Agents* encourages heterogeneous yet complementary evidence accumulation, thereby improving both the reliability and interpretability of the final decision.

3.2.5. Arbiter Agent

The *Arbiter Agent* serves as the final decision-maker of FetUSAgents. It integrates the evidence consolidated in the Evidence bank (Sec. E) and produces the final prediction \hat{y} .

3.2.6. Report Generator Agent

The *Report Generator Agent* synthesizes the evidence accumulated throughout the pipeline into a structured clinical report, as detailed in Sec. E(3).

3.3. Task-Specific Tool Library

The task-specific tool library (Fig. 1 B) covers three categories of fetal ultrasound analysis: plane classification, anatomical segmentation, and fetal biometry. *Expert Agents* (Sec. B) invoke the relevant tool subset and apply task-appropriate fusion rules to produce unified predictions.

3.3.1. Plane Classification

Accurate recognition of standard fetal planes is a prerequisite for reliable ultrasound interpretation. Four complementary classification tools for recognizing standard fetal views (i.e., head, abdomen, femur, and thorax) as well as three fetal brain sub-planes (i.e., trans-cerebellar, trans-thalamic, and trans-ventricular) are provided: (i) FetalCLIP (Maani et al., 2025), a vision-language foundation model that provides robust representations for fetal ultrasound images; (ii) a ResNet-50 backbone initialized with RadImageNet (Mei et al., 2022) weights and equipped with a classification head; (iii) FU-LoRA (Wang et al., 2024), a latent diffusion model fine-tuned via Low-Rank Adaptation (LoRA) (Hu et al., 2022); and (iv) a Vision Transformer

(ViT-B/16)(Dosovitskiy et al., 2021) initialized with ImageNet-1K(Deng et al., 2009) weights and equipped with a classification head. The corresponding *Expert Agent* applies agreement-based fusion for standard plane recognition and majority voting for brain sub-plane classification.

3.3.2. Anatomical Segmentation

Fine-grained anatomical segmentation accurately localizes and delineates fetal structures, underpinning subsequent biometric measurement. The tool library provides segmentation tools organized by anatomical region. Specifically, for fetal head segmentation, three complementary tools are provided: (i) CSM(Zeng et al., 2022), a lightweight CNN-based segmentation model; (ii) nnU-Net(Isensee et al., 2021), a self-configuring medical image segmentation framework; and (iii) the Ultrasound Foundation Model (USFM)(Jiao et al., 2024), adapted to this task by attaching and fine-tuning a segmentation head. The *Expert Agent* fuses the three mask outputs via pixel-level majority voting. For abdominal segmentation, two tools are provided: (i) FetalCLIP(Maani et al., 2025) and (ii) SAMUS(Lin et al., 2024), an interactive SAM-based ultrasound segmentation model. A sequential pipeline is employed as the fusion strategy: FetalCLIP first produces a coarse initial mask, from which the largest connected component and its centroid are extracted to form the input prompt (bounding box and point) for SAMUS. For fetal stomach segmentation, three tools are provided: (i) nnU-Net(Isensee et al., 2021), (ii) FetalCLIP(Maani et al., 2025), and (iii) SAMUS(Lin et al., 2024). The *Expert Agent* applies mask-level majority voting, followed by ordered fallback when the fused mask is unreliable.

3.3.3. Fetal Biometry

Fetal biometry quantifies fetal growth and anatomy, underpinning developmental assessment and clinical decision-making. The tool library supports routine biometric tasks. Specifically, for angle of progression (AoP) measurement, three tools are provided: (i) AoP-SAM(Zhou et al., 2025), a tailored SAM-based model for pubic symphysis and fetal head segmentation; (ii) USFM(Jiao et al., 2024); and (iii) an adapted UperNet(Xiao et al., 2018) model. The *Expert Agent* applies a median-guided outlier-correction rule as the fusion strategy. For gestational age (GA) estimation, three tools are provided: (i) FetalCLIP(Maani et al., 2025), along with two RadImageNet(Mei et al., 2022)-initialized backbones equipped with classification heads, namely (ii) ResNet-50 and (iii) ConvNeXt-Tiny(Liu et al., 2022). The *Expert Agent*

integrates the tool predictions using a consistency-aware weighted strategy. For HC and AC measurements, no additional dedicated tools are required. HC and AC are deterministically derived by ellipse fitting from the high-fidelity segmentation masks produced by the head and abdominal segmentation tools. The *Expert Agent* applies a priority-based fallback strategy to ensure robust HC and AC measurements when a preferred tool fails.

3.4. Deliberative VQA for Specific Tasks

The *Specific Tasks* branch handles fetal ultrasound VQA queries with explicit questions and candidate options (Fig. 1(c)), e.g., *Does this scan represent the trans-thalamic plane? (A) Yes (B) No*. The *Coordinator Agent* (Sec. B) routes such queries to this workflow, identifies the task type t , and selects the corresponding expert subset E_{selected} for tool invocation. The *Analyst Agent* (Sec. B) then transforms the user query \mathcal{Q} , candidate option set \mathcal{O} , and input image I into a structured question context shared with downstream agents:

$$A = \text{Analyst}(\mathcal{Q}, \mathcal{O}, I). \quad (2)$$

To combine interpretable reasoning evidence with reliable tool-supported evidence, a DPEA mechanism is proposed, comprising a deliberative path that captures diverse diagnostic reasoning from multiple LLM-based voters, and a computational path that provides structured predictions from task-specific tools.

In the deliberative path, five *Voter Agents* with distinct reasoning profiles (Sec. B) are deployed. This design is inspired by multidisciplinary team (MDT) consultation in clinical practice, where complementary expert perspectives are integrated for case-level decision making (Grembowski et al., 2014). Each voter independently examines the same case and produces both an option prediction and a textual rationale, thereby yielding diverse yet complementary reasoning evidence. Specifically, each voter independently produces a prediction–rationale pair, and the complete deliberative evidence set is:

$$E_{\text{vote}} = \{(l_j, r_j)\}_{j=1}^5, \quad (l_j, r_j) = V_j(\mathcal{Q}, \mathcal{O}, I, A), \quad (3)$$

where $l_j \in \mathcal{O}$ denotes the predicted option label and r_j the corresponding rationale.

In parallel, the computational path invokes the selected task-specific *Expert Agents* according to task type t and performs precise tool-based inference on the input image. Each expert communicates with the rest of

the system exclusively through structured JSON outputs, thereby reducing subjective free-form intermediate generation and improving factual reliability. Specifically, the complete computational evidence set is:

$$E_{\text{tool}} = \{(\hat{o}_k, \mathcal{D}_k)\}_{E_k \in E_{\text{selected}}}, \quad (\hat{o}_k, \mathcal{D}_k) = E_k(I), \quad (4)$$

where \hat{o}_k denotes the fused prediction of expert E_k and \mathcal{D}_k the associated decision details (e.g., measurements or intermediate structured evidence).

The final prediction is produced by the *Arbiter Agent*, which also receives the aggregated Evidence bank M (Sec. E). By jointly evaluating the consistency, complementarity, and relative strength of the two evidence paths, the *Arbiter Agent* ensures that neither pure language reasoning nor pure computational prediction dominates in isolation, yielding decisions that are both data-grounded and clinically interpretable.

3.5. Evidence Integration and Report Generation

Reliable fetal ultrasound report generation requires coherent integration of multi-source clinical evidence, multi-agent reasoning, and external medical knowledge. To this end, FetUSAgents combines retrieval-augmented external knowledge with a unified Evidence bank that consolidates heterogeneous evidence across the pipeline (Fig. 1(d)), serving both the specific-task (Sec. D) and general-task (Sec. F) workflows.

3.5.1. Retrieval-Augmented Generation

Retrieval-augmented generation (RAG)(Zakka et al., 2024) (Fig. 1(d), left) is incorporated to provide external medical evidence. Specifically, an external knowledge base is curated from authoritative references, including WHO guidelines(Kiserud et al., 2017) and ISUOG practice standards, which provide guidance for standard plane acquisition, anatomical landmark identification, biometric measurement, and clinical interpretation in fetal ultrasound. All reference documents are split into semantically coherent chunks $K = \{k_i\}_{i=1}^N$ and embedded into a shared vector space via a pretrained encoder $f_{\theta}(\cdot)$. Given a query Q , the system retrieves the top- k most relevant snippets as external medical evidence:

$$E_{\text{rag}} = \text{Retrieve}(Q, K) = \{k_i\}_{i=1}^k, \quad (5)$$

which informs both the *Arbiter Agent*'s decision and the subsequent report generation.

3.5.2. Evidence bank

In a multi-agent pipeline, clinically meaningful reports must coherently integrate anatomical observations, quantitative measurements, multi-agent reasoning, and external medical knowledge. However, these evidence sources are distributed across heterogeneous modules and may be only partially preserved during free-form text synthesis. To address this issue, FetUSAgents introduces a unified Evidence bank to aggregate intermediate evidence from multiple sources:

$$M = \{A, E_{\text{vote}}, E_{\text{tool}}, E_{\text{rag}}\}. \quad (6)$$

For the specific-task workflow, all four components are populated as described in Sec. D and Sec. E (1). For the general-task workflow (Sec. F), where no explicit candidate options or voter deliberation are involved, the Evidence bank reduces to

$$M_{\text{gen}} = \{A, E_{\text{tool}}, E_{\text{rag}}\}, \quad (7)$$

retaining the tool evidence and retrieved knowledge to support report generation.

3.5.3. Report Generation

Based on the aggregated evidence, the *Report Generator Agent* consolidates the Evidence bank M together with the final prediction \hat{y} from the *Arbiter Agent* to produce the structured clinical report, which comprises three sections: (i) *Findings*, which objectively describe observable anatomical structures and image features; (ii) *Impression*, which summarizes the final clinical interpretation; and (iii) *Note*, which provides a summary of the supporting evidence.

3.6. End-to-End Clinical Workflow for General Tasks

The *General Tasks* branch addresses open-ended requests (Fig. 1(e)) and covers two sub-tasks: *image caption generation* (e.g., “Generate a caption for this ultrasound image”) and *video summarization* (e.g., “Summarize the key findings in this ultrasound video”). Given a user query Q , once the *Coordinator Agent* routes the case to this branch, it further identifies which sub-task the request belongs to.

3.6.1. Image Caption Generation.

For open-ended image queries, FetUSAgents identifies the anatomical plane and activates the corresponding *Expert Agents* to extract anatomical

observations and quantitative measurements. Beyond this standard pipeline, a WHO-chart-based internal consistency check (Kiserud et al., 2017) is introduced to prevent contradictory reporting by correlating derived biometric indices (e.g., HC, AC) with the estimated GA to compute normative growth percentiles. When a measurement falls outside clinically plausible ranges, a reflection step re-evaluates the expert outputs and replaces unreliable estimates with robust ensemble fallbacks. The verified findings are then consolidated into a structured report via *Report Generator Agent* with the Evidence bank.

3.6.2. Video Summarization.

In a continuous ultrasound stream $V = \{I_t\}_{t=1}^T$, only a small fraction of frames contain standardized diagnostic views. FetUSAgents deploys a keyframe extractor based on FetalCLIP (He et al., 2025) to automatically isolate and classify clinically meaningful planes, which are then dispatched to the corresponding *Expert Agents* for frame-wise analysis. The resulting multi-frame evidence is aggregated via the Evidence Bank and *Report Generator Agent* into a cohesive, sequence-level clinical summary that captures key anatomical and biometric findings across the entire examination. This pipeline mirrors the real-world sonographer workflow of scanning, identifying key views, measuring, and synthesizing findings, thereby offering a clinically practical solution for open-ended fetal ultrasound interpretation.

4. Experiment

4.1. Datasets and FetUS-VQA Construction

4.1.1. Overview

Our experiments employ 10 publicly available datasets covering 7 clinically relevant tasks (Fig. 2). For each task, one dataset is used to train the visual tools within the Expert Agents, while an independently collected counterpart is reserved for OoD evaluation, ensuring cross-institutional generalization. The OoD evaluation sets additionally serve as the image source for the FetUS-VQA (Sec. 4.1.4).

4.1.2. Task-Specific Datasets

(i) *Abdominal Circumference (AC) Estimation*: The ACOUSLIC-AI (Sapia et al., 2025) dataset was used for training, which contains 252,000 blind-sweep ultrasound images, among which 6,620 images with abdominal annotations were selected. For OoD evaluation, AC-Data (Ashkani Chenarlogh

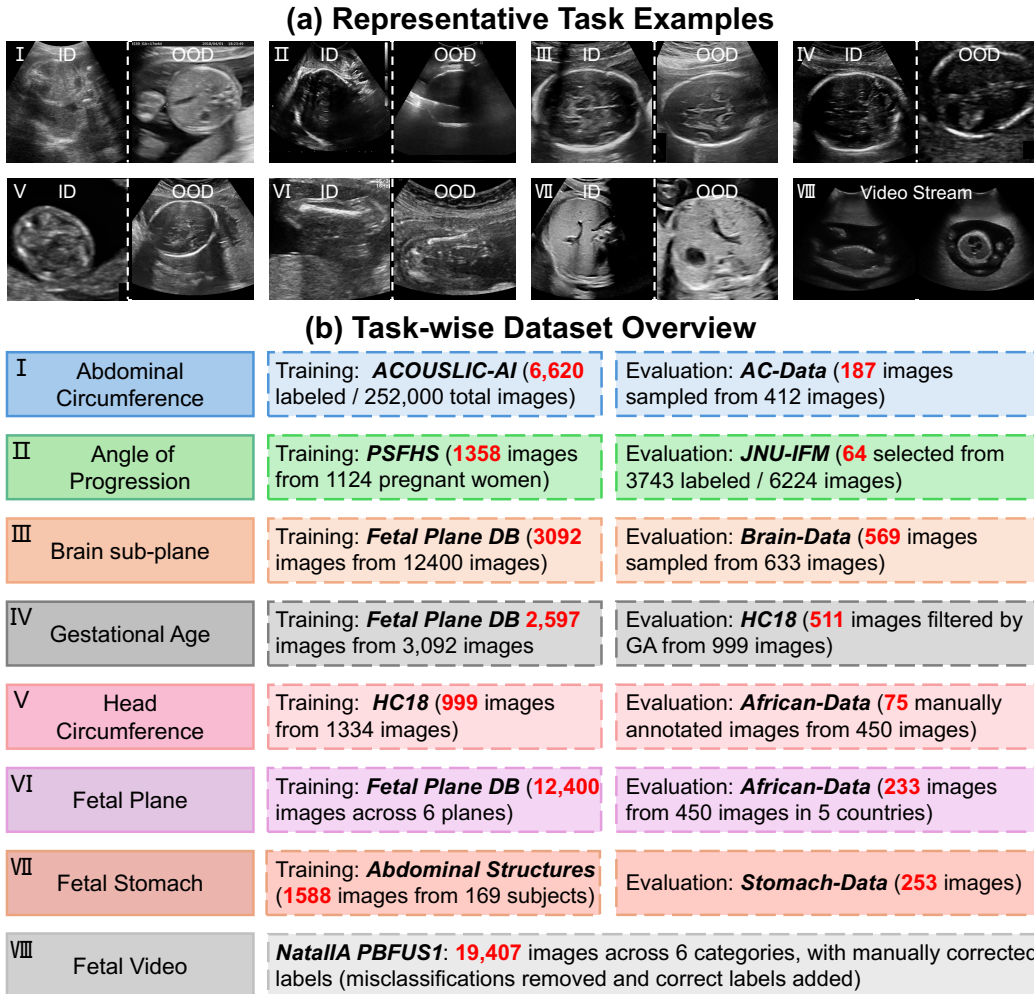


Figure 2: Overview of datasets and tasks. (a) Representative in-distribution (ID) and out-of-distribution (OoD) image pairs for each task. (b) Task-wise summary of training and evaluation datasets.

et al., 2022) provides 412 images, from which 187 images were selected. (ii) *Angle of Progression (AoP Estimation)*: The PSFHS (Chen et al., 2024a) dataset (1,358 images) was used for training. For OOD evaluation, 64 labeled images from different videos in JNU-IFM (Lu et al., 2022) (6,224 images, 3,743 labeled) were used. (iii) *Brain Sub-plane Classification*: The brain subset of Fetal Plane DB (Burgos-Artizzu et al., 2020b) (3,092 images: 1,638 trans-thalamic, 714 trans-cerebellar, 597 trans-ventricular, and 143 other) was used for training. For OOD evaluation, 569 selected images (90 trans-

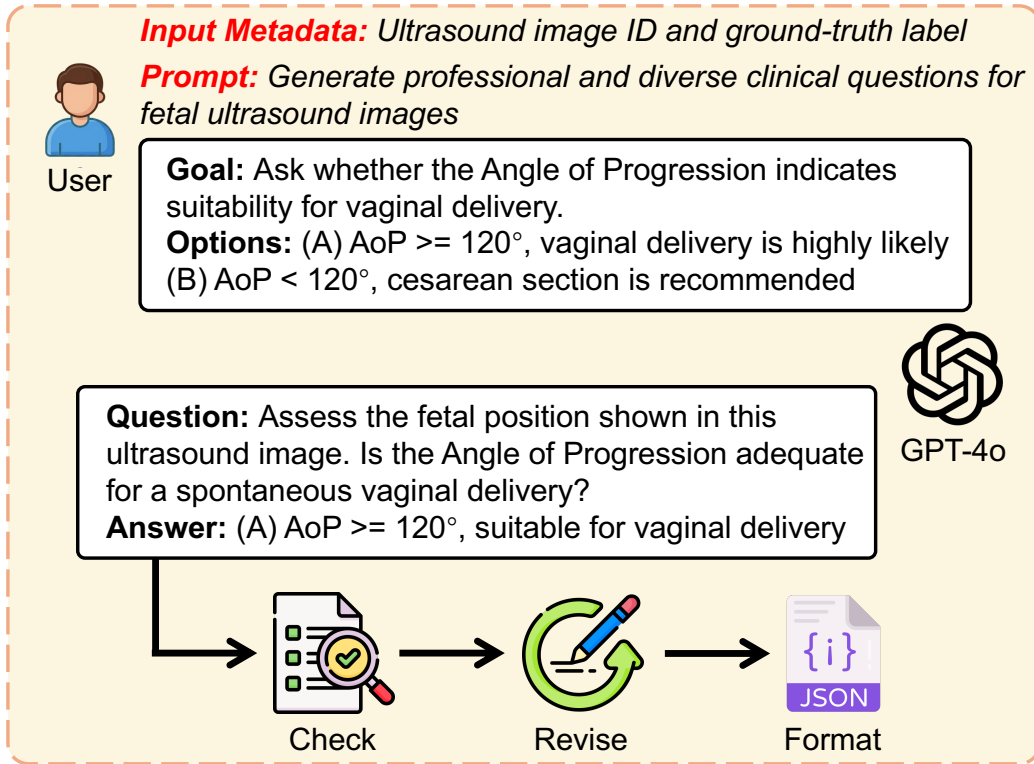


Figure 3: Semi-automated pipeline for FetUS-VQA construction. Given an image ID and its ground-truth label, a task-aware prompt guides GPT-4o to generate clinically grounded question-answer pairs, which then undergo expert checking, revision, and standardized JSON formatting.

cerebellar, 228 trans-thalamic, 251 trans-ventricular) from 633 Brain-Data (Belciug, 2024) images were used. (iv) *Gestational Age (GA) Estimation*: The Fetal Plane DB (Burgos-Artizzu et al., 2020b) dataset (2,597 brain images) was used for training, and 511 brain images from HC18 (van den Heuvel et al., 2018) were used for OOD evaluation. As neither dataset provides GA annotations, following FetalCLIP (Maani et al., 2025), HC is first computed from the segmentation masks and then converted to GA via numerical inversion of the WHO fetal growth model. (v) *Head Circumference (HC) Estimation*: The HC18 (van den Heuvel et al., 2018) dataset (1,334 images total) was used for training, from which 999 brain images were selected. For OOD evaluation, 75 images with manual annotations (Wang et al., 2024) were selected from the African-Data (Sendra-Balcells et al., 2023) dataset. (vi) *Plane Classification*: The full Fetal Plane DB (Burgos-Artizzu et al., 2020b)

dataset (12,400 images: 711 abdomen, 3,092 brain, 1,040 femur, 1,718 thorax, 1,626 cervix, and 4,213 other) was used for training. For OoD evaluation, the African-Data (Sendra-Balcells et al., 2023) dataset (125 abdomen, 125 brain, 125 femur, and 75 thorax) was used. (vii) *Stomach Segmentation*: The Abdominal Structures (Belciug, 2024) dataset (1,588 images) was used for training and Stomach-Data (Da Correggio et al., 2023) (253 images) was used for OOD evaluation.

4.1.3. Video Summarization Dataset

For video-level summarization evaluation, the public fetal ultrasound video dataset Natalia PBFUS1 (González et al., 2024) is adopted, containing 19,407 frames in total. The original frame-level annotations were revised by one experienced physician, yielding 47 Biparietal Plane, 78 Abdominal Plane, 68 Heart Plane, 139 Spine Plane, 47 Femur Plane, and 19,028 No Plane frames.

4.1.4. FetUS-VQA Construction

To enable end-to-end assessment of multimodal reasoning, FetUS-VQA was constructed from the OoD evaluation datasets as the first VQA benchmark dedicated to fetal ultrasound. It comprises 1,892 images and 3,205 question-answer pairs across 10 clinical tasks (Table 1). Specifically, FetUS-VQA is built via a semi-automated pipeline (Fig. 3). For each image, its identifier and ground-truth label are fed into a task-aware prompt that guides GPT-4o to generate clinically grounded question-answer pairs. For classification tasks, the label serves as the correct option with the remaining class labels as distractors. Each such task is further formulated in both binary (e.g., “Does this scan represent the trans-thalamic plane? (A) Yes (B) No”) and multi-class (e.g., “Identify the cranial plane in this fetal brain ultrasound: (A) Trans-cerebellum, (B) Trans-thalamic, (C) Trans-ventricular”) formats to probe robustness under varying diagnostic difficulty. For measurement tasks, a quantitative value (e.g., circumference in mm, angle in degrees, or area in cm^2) is computed from the segmentation mask and discretized into candidates at clinically meaningful intervals. All generated pairs undergo expert review to ensure clinical accuracy and answer validity, and the finalized benchmark is released in standardized JSON format.

4.2. Comparative MLLMs

For comprehensive evaluation, we benchmark FetUSAgents against a diverse set of baseline MLLMs, including both general models (i.e., GPT-5.1(OpenAI, 2025), GPT-5.4(OpenAI, 2026a), Qwen3-Max(Qwen Team,

Table 1: Overview of the FetUS-VQA benchmark.

Dataset Overview				
Fetal ultrasound images				1,892
VQA pairs				3,205
Question Taxonomy				
Category	ID	Task	Options	VQA pairs
Measurement	Task1	AC	4 (A/B/C/D)	187
	Task2	AoP	2 (A/B)	64
	Task9	HC	4 (A/B/C/D)	75
	Task10	Stomach	4 (A/B/C/D)	253
	Subtotal	4 tasks		579
Classification	Task3	Brain Binary	2 (A/B)	569
	Task4	Brain Multi	3 (A/B/C)	569
	Task5	Plane Binary	2 (A/B)	233
	Task6	Plane Multi	4 (A/B/C/D)	233
	Task7	GA Binary	2 (A/B)	511
	Task8	GA Multi	3 (A/B/C)	511
	Subtotal	6 tasks		2,626
Total		10 tasks		3,205

2025), Qwen3-VL-30B-A3B(Bai et al., 2025), DeepSeek-V3.2(DeepSeek-AI et al., 2025), Doubao-Seed-2.0-Pro(ByteDance Seed, 2026), and Gemini-3-Flash-Preview-Thinking(Google DeepMind, 2025)) and medical models (i.e., LLaVA-Med-v1.5-Mistral-7B(Li et al., 2023), HuatuoGPT-34B(Chen et al., 2024b), Hulu-Med-30A3(Jiang et al., 2025), Hulu-Med-32B(Jiang et al., 2025), and MedGemma-27B(Sellergren et al., 2025)).

4.3. Implementation Details

All experiments were conducted on a workstation equipped with a single NVIDIA A800 GPU with 80 GB VRAM. All LLM-driven agents in FetUSAgents used GPT-5.1(OpenAI, 2025) as the language-model backbone.

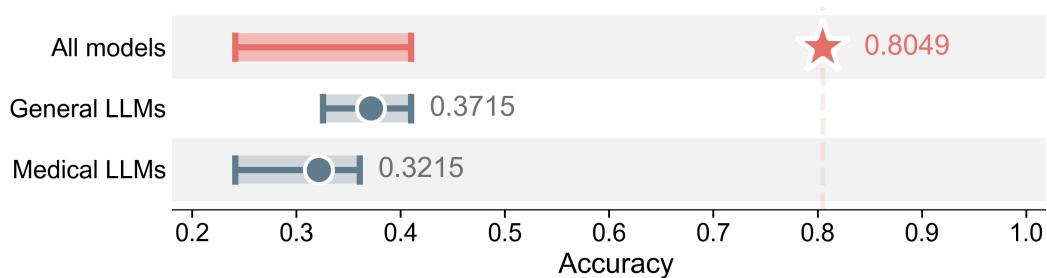


Figure 4: VQA accuracy on measurement tasks. Circles: group means; bars: ranges; stars: FetUSAgents.

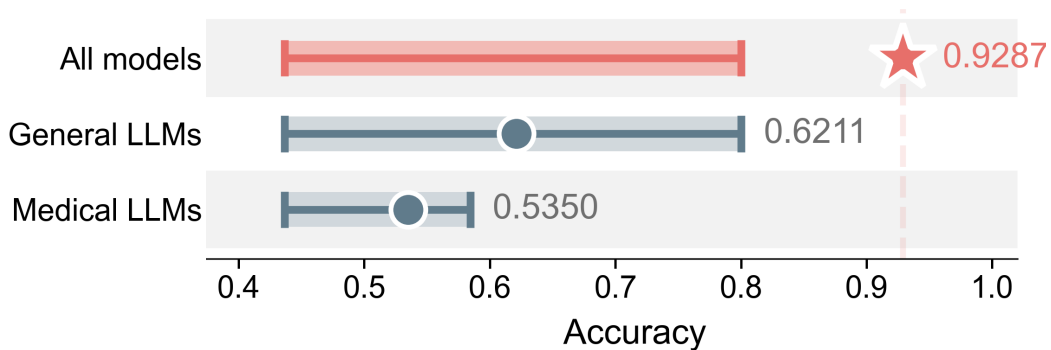


Figure 5: VQA accuracy on classification tasks. Circles: group means; bars: ranges; stars: FetUSAgents.

For RAG, a knowledge base was constructed using Chroma as the persistent vector database. Reference documents were embedded using OpenAIEmbeddings(LangChain, 2026) with the text-embedding-3-small(OpenAI, 2026b) embedding model. During inference, FetUSAgents retrieved the top 5 most relevant knowledge snippets for each query.

4.4. Comparison with MLLMs on FetUS-VQA

FetUSAgents consistently outperformed all general and medical MLLMs on the FetUS-VQA benchmark in both accuracy and macro-F1 score (Tables 2 and 3). Specifically, FetUSAgents achieved an average accuracy of 0.8791 and an average macro-F1 score of 0.8721, surpassing the strongest general baseline, Gemini-3-Flash-Thinking (accuracy, 0.6272; macro-F1, 0.5509), by 25.19% and 32.12%, and the best medical baseline, Hulu-Med-32B (accuracy, 0.4941; macro-F1, 0.4493), by 38.50% and 42.28%, with this superiority maintained across all ten tasks. FetUSAgents also exhibited well-balanced class-wise predictions, with closely aligned accuracy and macro-F1 scores, whereas most

Table 2: VQA accuracy (%) on the FetUS-VQA benchmark. Best results are in **bold** and runner-up underlined. “Rand”: the random-guess baseline.

Method	Task1	Task2	Task3	Task4	Task5	Task6	Task7	Task8	Task9	Task10	Avg.
Rand	0.2500	0.5000	0.5000	0.3333	0.5000	0.2500	0.5000	0.3333	0.2500	0.2500	0.3667
(a) General large language models											
GPT-5.1	0.3048	0.5469	0.5501	0.3533	0.7425	0.6781	0.8160	0.6986	0.3867	0.2767	0.5354
GPT-5.4	0.3262	0.4688	0.5641	0.4112	0.7854	0.7511	0.8043	<u>0.8278</u>	0.4000	0.1067	0.5446
Qwen3-MAX	0.4439	0.5938	0.5009	0.3831	0.4936	0.2790	0.2505	0.7123	0.2933	0.3083	0.4259
Qwen3-VL-30B-A3B	<u>0.4599</u>	0.4062	0.5026	0.4183	0.6266	0.4893	0.4090	0.7456	0.3333	0.3320	0.4723
DeepSeek-V3.2	0.2995	0.4531	0.5009	0.4007	0.4807	0.2790	0.7456	0.7358	0.2933	0.2767	0.4465
Doubao-Seed-2.0-Pro	0.4492	0.5312	0.6204	0.5817	0.8240	0.7639	<u>0.8356</u>	0.7241	0.3333	0.3083	0.5972
Gemini-3-Flash-Thinking	0.3209	0.5000	<u>0.7100</u>	<u>0.7311</u>	<u>0.9185</u>	<u>0.9056</u>	0.7828	0.7534	<u>0.4400</u>	0.2095	0.6272
(b) Medical large language models											
Llava-Med-V1.5-Mistral-7B	0.1979	0.5938	0.4148	0.4411	0.4893	0.2747	0.2544	0.7456	0.2400	0.2688	0.3960
HuatuogPT-34B	0.1925	0.3594	0.5413	0.4341	0.6438	0.3734	0.3659	0.6301	0.2000	0.2134	0.3954
Hulu-Med-30A3	0.3690	0.4375	0.5888	0.4060	0.6309	0.7167	0.3875	0.7456	0.2400	0.2411	0.4763
Hulu-Med-32B	0.3422	0.5626	0.5975	0.4183	0.7039	0.6009	0.4364	0.7495	0.2133	<u>0.3162</u>	0.4941
MedGemma-27B	0.2567	<u>0.6250</u>	0.5729	0.4464	0.5708	0.3777	0.7456	0.7456	0.2800	0.2806	0.4901
FetUSAgents	0.9947	0.7188	0.9332	0.9086	0.9399	0.9313	0.9295	0.9295	1.0000	0.5059	0.8791

baselines showed lower macro-F1 than accuracy, indicating biased category preferences. Notably, when accuracy is disaggregated by task category (Figs. 4 and 5), baseline MLLMs scored substantially lower on measurement tasks (0.2–0.5) than on classification tasks (0.4–0.8), revealing that current models remain more capable of semantic recognition than geometric quantification. FetUSAgents, by contrast, exceeded 0.80 accuracy on both measurement (0.8049) and classification (0.9287) tasks, effectively bridging this gap. General MLLMs consistently outperformed their medical counterparts, suggesting that fine-tuning with limited medical corpora does not necessarily confer advantages in fetal ultrasound.

4.5. Comparison with MLLMs on Report Generation

Beyond VQA accuracy, report generation quality (Fig. 6) was assessed from two complementary perspectives: (i) LLM-based evaluation, in which Gemini-3-Pro-Thinking(Google, 2025) scores each report on a 1–5 scale across five dimensions (i.e., *Clinical Accuracy*, *Completeness*, *Reasoning*, *Professional Language*, and *Overall Quality*), with a reference image description automatically constructed from contextual information (Fig. 8) as auxiliary evaluation context; and (ii) expert evaluation, in which two clinical sonographers independently rate the same reports on a 1–5 scale across four dimensions (i.e., *Accuracy*, *Completeness*, *Professional Language*, and *Structural Organization*). For both evaluations, each model’s score is normalized by that of GPT-5.4 to

Table 3: VQA macro-F1 score on the FetUS-VQA benchmark. Best results are in **bold** and runner-up underlined.

Method	Task1	Task2	Task3	Task4	Task5	Task6	Task7	Task8	Task9	Task10	Avg.
(a) General large language models											
GPT-5.1	0.2880	0.5205	0.5484	0.3401	0.7419	0.6420	0.7498	0.3207	0.3434	0.2560	0.4751
GPT-5.4	0.3165	0.4688	0.5500	0.3866	0.7805	0.7176	<u>0.7685</u>	<u>0.7033</u>	0.3261	0.1021	0.5120
Qwen3-MAX	<u>0.4297</u>	0.3725	0.3368	0.2416	0.4070	0.1094	0.2020	0.2789	0.2651	0.2590	0.2902
Qwen3-VL-30B-A3B	0.4073	0.3091	0.3928	0.2980	0.6194	0.3590	0.4026	0.4271	0.2975	0.2789	0.3792
DeepSeek-V3.2	0.2449	0.4465	0.3337	0.1976	0.4782	0.1630	0.4271	0.2826	0.1947	0.2148	0.2983
Doubao-Seed-2.0-Pro	0.4078	0.5271	0.6202	0.4638	0.8197	0.6906	0.7285	0.2901	0.3321	<u>0.2968</u>	0.5177
Gemini-3-Flash-Thinking	0.3148	0.3592	<i>0.7012</i>	<u>0.6893</u>	<u>0.9184</u>	<u>0.8803</u>	0.5779	0.4589	<u>0.4149</u>	0.1939	<u>0.5509</u>
(b) Medical large language models											
Llava-Med-V1.5-Mistral-7B	0.1796	0.3725	0.4071	0.2041	0.3378	0.1747	0.2028	0.4271	0.1253	0.1182	0.2549
HuatuoGPT-34B	0.1789	0.3580	0.4781	0.2918	0.6431	0.2753	0.3591	0.5679	0.1771	0.2043	0.3534
Hulu-Med-30A3	0.2944	0.4325	0.5887	0.1995	0.5830	0.6345	0.3874	0.4271	0.1556	0.1557	0.3858
Hulu-Med-32B	0.3248	<u>0.5586</u>	0.5601	0.2762	0.7038	0.5407	0.4364	0.5928	0.2042	0.2949	0.4493
MedGemma-27B	0.1762	0.5194	0.5691	0.2632	0.5690	0.3054	0.4271	0.4271	0.1491	0.2284	0.3634
FetUSAgents	0.9942	0.7046	0.9332	0.8958	0.9396	0.9277	0.9102	0.9102	1.0000	0.5051	0.8721

Table 4: LLM-based evaluation of report generation quality. Each score is the average across five dimensions (Clinical Accuracy, Completeness, Reasoning, Professional Language, and Overall Quality), normalized relative to GPT-5.4. For tasks with both binary and multi-class variants, only the multi-class setting is evaluated. Best results are in **bold** and runner-up underlined.

Method	AC	AoP	Brain	Plane	GA	HC	Stomach	Avg.
(a) General large language models								
GPT-5.1	0.9760	<u>1.0290</u>	0.8942	0.9110	1.0101	0.8762	1.1483	0.9778
GPT-5.4	1.0000	1.0000	1.0000	1.0000	1.0000	<u>1.0000</u>	1.0000	1.0000
Qwen3-Max	<u>1.0442</u>	0.9523	0.9870	0.6134	0.9259	0.9187	1.2165	0.9511
Qwen3-VL-30B-A3B	1.0303	0.9680	0.9087	0.7384	1.0067	0.9285	<u>1.2502</u>	0.9758
DeepSeek-V3.2	1.0236	0.9404	0.7233	0.5950	0.7499	0.9235	1.1690	0.8750
Doubao-Seed-2.0-Pro	0.9669	0.9212	0.5541	0.9128	0.5009	0.9083	0.7745	0.7912
Gemini-3-Flash-Preview-Thinking	0.8592	0.9852	<u>1.1785</u>	1.0709	<u>1.0215</u>	0.9234	1.0834	<u>1.0174</u>
(b) Medical large language models								
LLaVA-Med-v1.5-Mistral-7B	0.8247	0.9189	0.5038	0.5305	0.4518	0.7334	1.0154	0.7112
HuatuoGPT-34B	0.8726	0.9323	0.8619	0.6356	0.9211	0.8710	1.1353	0.8900
Hulu-Med-30A3	1.0301	0.8983	0.9026	0.8883	0.9731	0.8441	1.1107	0.9496
Hulu-Med-32B	0.9251	0.9268	0.8780	0.8156	0.9589	0.8705	1.1778	0.9361
MedGemma-27B	0.9222	0.9479	0.8259	0.7504	0.9553	0.9240	1.2070	0.9332
FetUSAgents	1.2418	1.1765	1.3138	<u>1.0120</u>	1.0743	1.2398	1.2928	1.1930

yield a relative score.

For LLM-Based evaluation, FetUSAgents consistently outperformed all baselines, achieving an average relative score of 1.1930 (+19.30% over GPT-5.4), compared with the strongest general baseline Gemini-3-Flash-Preview-



Figure 6: Representative examples of report generation across seven VQA tasks. The yellow boxes show the input VQA questions, the red boxes present the reports generated by the best baseline model, and the blue boxes show the reports generated by FetUSAgents. The undesired and desired responses are highlighted in red and green respectively.

Thinking (1.0174) and the strongest medical baseline Hulu-Med-30A3 (0.9496), yielding further improvements of 17.26% and 25.63%, respectively. Radar chart analysis (Fig. 7(a, b)) showed that the contour of FetUSAgents consistently

Table 5: Expert evaluation of report generation quality. Each score is the average across four dimensions (Accuracy, Completeness, Professional Language, and Structural Organization), normalized relative to GPT-5.4. For tasks with both binary and multi-class variants, only the multi-class setting is evaluated. Best results are in **bold** and runner-up underlined.

Method	AC	AoP	Brain	Plane	GA	HC	Stomach	Avg.
(a) General large language models								
GPT-5.1	1.1660	1.1156	1.0865	1.2198	1.1045	1.0882	0.9823	1.1090
GPT-5.4	1.0000	1.0000	1.0000	1.0000	1.0000	1.0000	1.0000	1.0000
Qwen3-Max	1.1826	0.9490	1.0163	1.1781	1.0083	1.2243	1.1229	1.0974
Qwen3-VL-30B-A3B	1.1676	1.0434	1.1017	1.2611	1.0278	1.2243	1.1250	1.1359
DeepSeek-V3.2	1.2052	<u>1.1701</u>	1.0823	1.1510	1.1205	1.1993	1.1031	1.1474
Doubao-Seed-2.0-Pro	1.0774	1.0104	1.1458	1.2344	1.1747	1.0378	1.1073	1.1125
Gemini-3-Flash-Preview-Thinking	1.0045	1.1330	<u>1.2240</u>	<u>1.3132</u>	<u>1.2076</u>	1.1722	1.0750	1.1614
(b) Medical large language models								
LLaVA-Med-v1.5-Mistral-7B	0.8913	0.9361	0.7712	0.8229	0.5365	0.9892	0.9715	0.8455
HuatuoGPT-34B	0.9799	0.8781	0.9410	0.9705	0.8497	0.9014	0.8417	0.9089
Hulu-Med-30A3	1.0785	0.8691	1.0976	1.1585	1.1517	1.1646	0.9427	1.0661
Hulu-Med-32B	1.1378	1.0278	1.0632	1.0488	1.0142	1.0000	0.8333	1.0179
MedGemma-27B	<u>1.2368</u>	1.1097	1.1587	1.2281	1.1243	1.2722	<u>1.2042</u>	<u>1.1906</u>
FetUSAgents	1.3170	1.3354	1.3306	1.4436	1.2944	<u>1.2507</u>	1.2573	1.3184

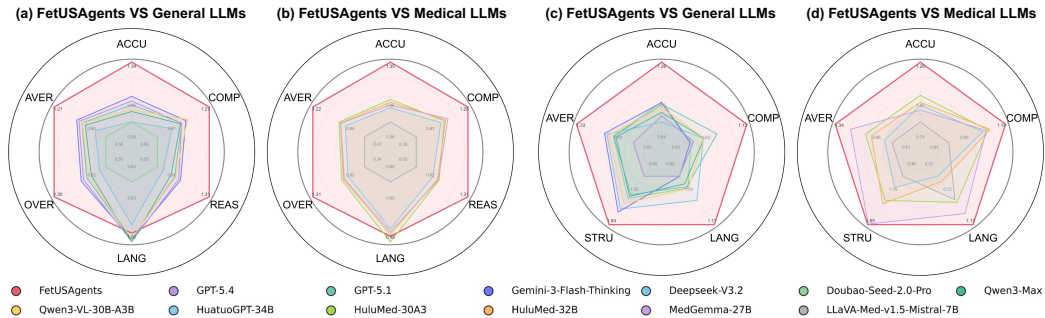


Figure 7: Radar-chart comparison of report generation quality. (a, b) LLM-based and (c, d) expert evaluation against general (a, c) and (b, d) LLMs. ACCU: Clinical Accuracy; COMP: Completeness; REAS: Reasoning; LANG: Professional Language; OVER: Overall Quality; STRU: Structural Organization; AVER: Dimension-averaged score.

enclosed those of all baselines, with the largest margins on dimensions tied to clinical grounding and reasoning and a relatively narrow gap on *Professional Language*, suggesting that current MLLMs can produce professionally phrased text but remain limited in integrating domain-specific evidence and performing structured clinical reasoning.

Expert evaluation further confirmed the superiority of FetUSAgents, which

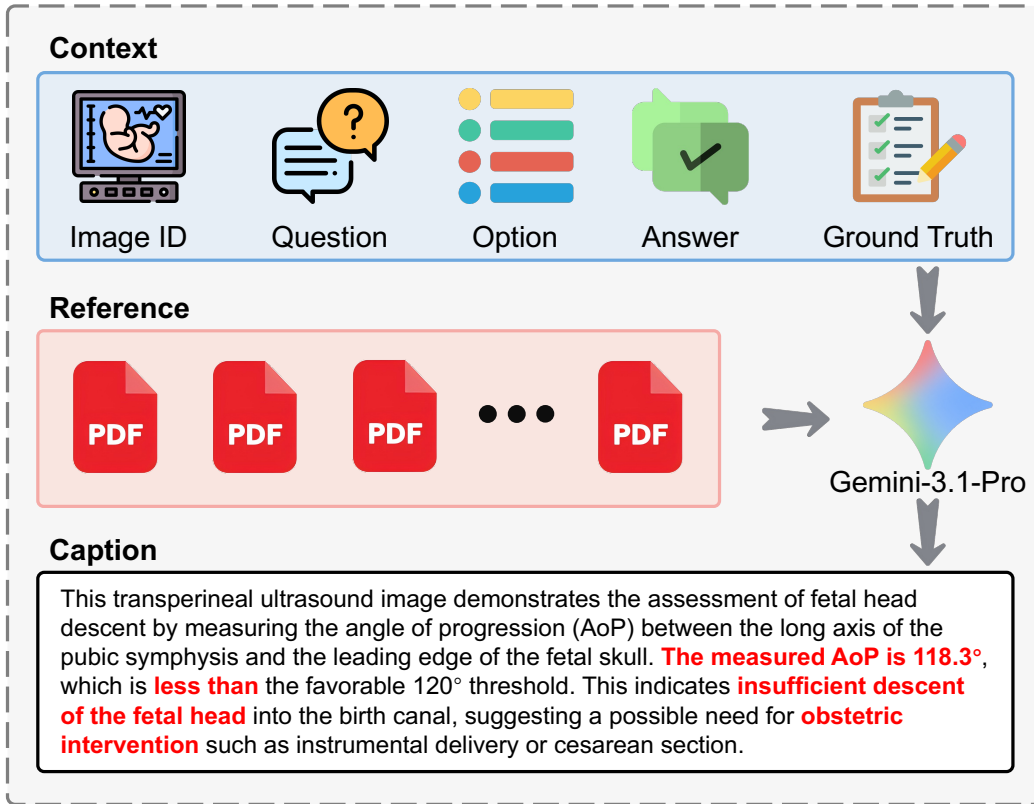


Figure 8: Reference caption construction for LLM-based report evaluation. Task-specific context (image ID, question, options, answer, and ground truth) together with external reference documents are provided to Gemini-3.1-Pro to synthesize clinically grounded reference descriptions.

achieved an average relative score of 1.3184 (+31.84% over GPT-5.4), exceeding Gemini-3-Flash-Preview-Thinking (1.1614) and MedGemma-27B (1.1906) by 13.52% and 10.73%, respectively. At the task level, FetUSAgents ranked first on six of seven tasks and second on HC, demonstrating consistent robustness. Radar chart analysis (Fig. 7(c, d)) showed that FetUSAgents again achieved the most balanced profile, with its contour enclosing all baselines across every expert-rated dimension, further supporting its clinical reliability for fetal ultrasound report generation.

4.6. Qualitative Evaluation on General Tasks

To complement the quantitative analyses above, the end-to-end output of FetUSAgents is qualitatively assessed on two representative general-task sce-

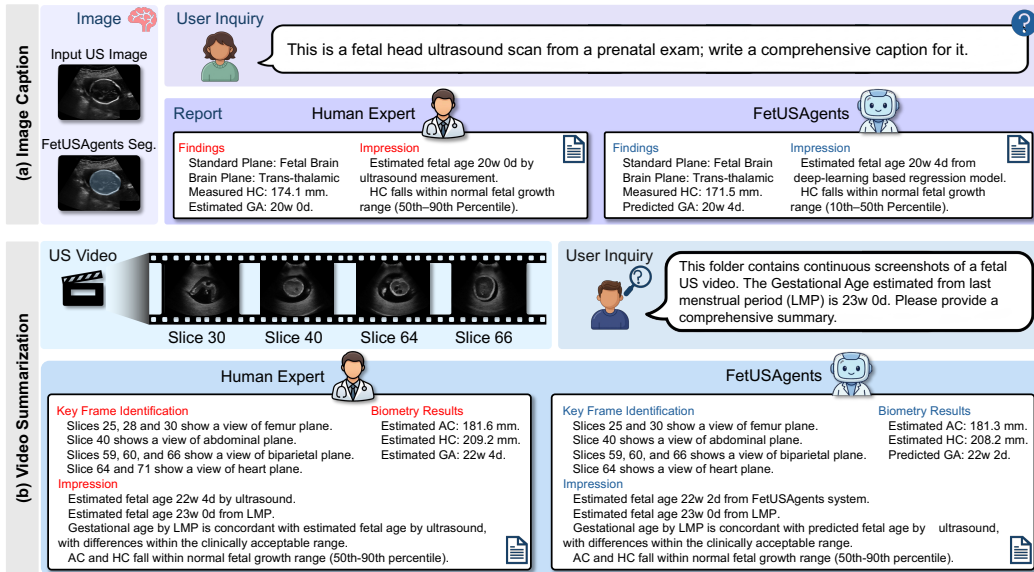


Figure 9: Qualitative examples of general-task outputs. (a) Image captioning: FetUSAgents identifies the standard plane, performs biometry, and produces a structured report closely aligned with the human expert reference. (b) Video summarization: FetUSAgents extracts multi-plane keyframes from a continuous scan and cross-validates ultrasound-derived GA against estimates based on the last menstrual period (LMP).

narios (Fig. 9). For single-image captioning, FetUSAgents correctly identified the trans-thalamic brain plane, invoked the corresponding Expert Agents to measure HC and estimate GA, and synthesized the anatomical and biometric findings into a structured report closely aligned with the expert reference. For video summarization, FetUSAgents automatically extracted clinically meaningful keyframes from a continuous scan, recognized the corresponding anatomical planes (femur, abdominal, biparietal, and heart views), aggregated frame-wise biometric evidence into a cohesive summary, and cross-validated the ultrasound-derived GA against the LMP-based estimate to verify clinical consistency. Across both scenarios, FetUSAgents exhibited high concordance with expert-provided references in plane identification, quantitative measurements, and final impression formulation, underscoring its capacity to approximate real-world sonographer workflows.

4.7. Comparison with Standalone Tools

To quantify the gain from multi-tool fusion, each *Expert Agent* was compared with the best-performing standalone tool on the corresponding task

FetUSAgents VS Best Tools

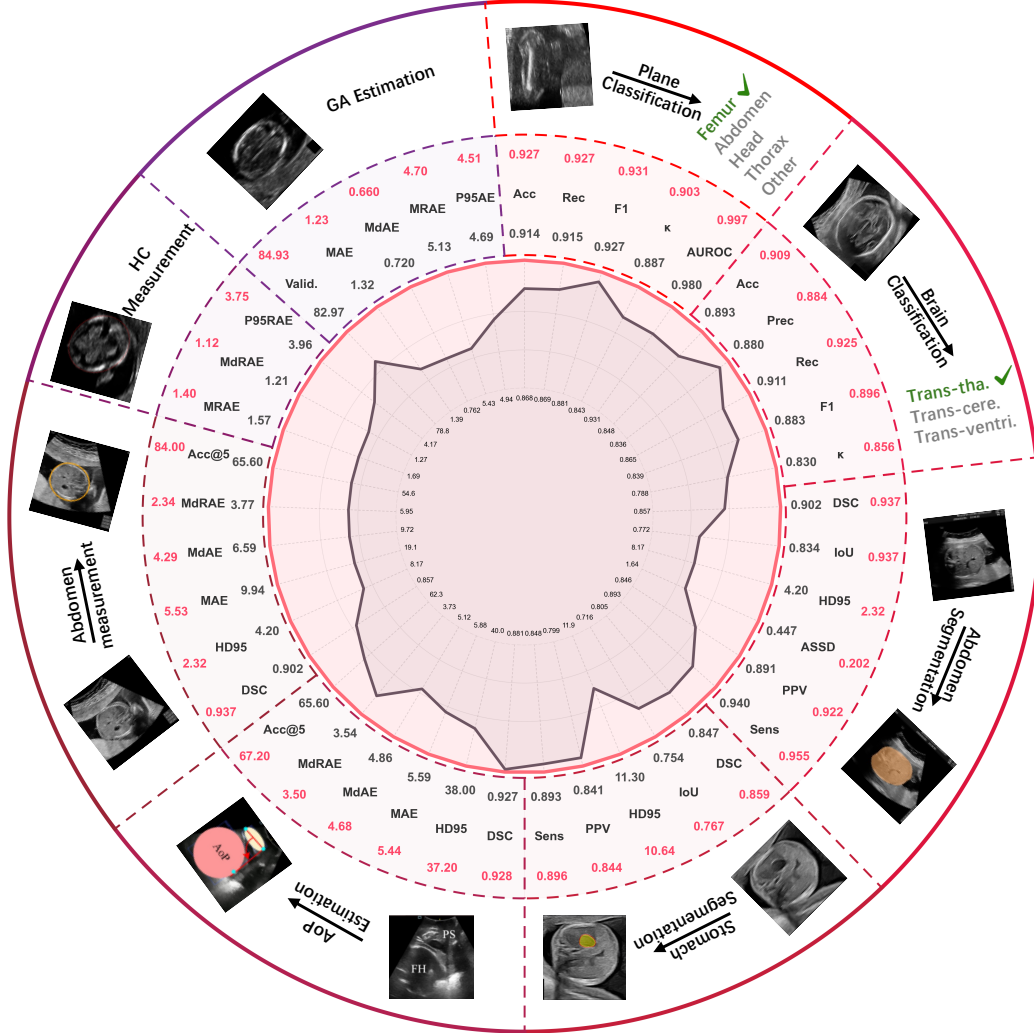


Figure 10: Radar-chart comparison of FetUSAgents (red curves and values) versus the best standalone tool (gray curves and values) across eight fetal ultrasound tasks. All metrics are normalized to a unified scale where the outer boundary consistently indicates superior performance. Abbreviations: Acc, accuracy; Prec, precision; Rec, recall; κ , Cohen’s kappa; DSC, Dice coefficient; IoU, intersection over union; HD95, 95th-percentile Hausdorff distance; ASSD, average symmetric surface distance; PPV, positive predictive value; Sens, sensitivity; MAE/MdAE, mean/median absolute error; MRAE/MdRAE, mean/median relative absolute error; P95AE/P95RAE, 95th-percentile absolute/relative error; Acc@5, accuracy within 5%; Valid., validity rate.

Table 6: Ablation study on VQA accuracy across three representative tasks.

Method	Task2	Task6	Task9	Avg
w/o Arbiter Agent	<u>0.6719</u>	0.8283	0.7467	0.7490
w/o Expert Agents	0.4063	<u>0.8884</u>	<u>1.0000</u>	<u>0.7649</u>
w/o DPEA	0.5936	0.7940	0.7467	0.7114
FetUSAagents	0.7188	0.9313	1.0000	0.8834

Table 7: Ablation study on report generation quality across three representative tasks.

Method	Task2	Task6	Task9	Avg
w/o Arbiter Agent	<u>1.1615</u>	0.9633	1.1420	<u>1.0889</u>
w/o Expert Agents	0.9666	0.9692	1.2480	1.0613
w/o DPEA	1.0113	0.9242	1.1274	1.0210
w/o Evidence bank	1.1529	<u>0.9749</u>	1.1238	1.0839
FetUSAagents	1.1765	1.0120	<u>1.2398</u>	1.1428

across all eight evaluation tasks (Fig. 10). Task-appropriate metrics were adopted: *Accuracy*, *Precision*, *Recall*, *F1*, *Cohen’s κ* , and *AUROC* for classification; *DSC*, *IoU*, *HD95*, *ASSD*, *PPV*, and *Sensitivity* for segmentation; *MAE*, *MdAE*, *MRAE/MdRAE*, *P95 AE/P95 RAE*, and *Acc@5%* for biometry, with an additional *Validity Rate* (Maani et al., 2025) for GA estimation. To enable joint visualization of these heterogeneous metrics in a single radar plot, all values were mapped to a unified scale where larger values consistently indicate better performance: for higher-is-better metrics, $x' = x / \max(x_{EA}, x_{tool})$; for lower-is-better metrics, $x' = \min(x_{EA}, x_{tool}) / x$, where x_{EA} and x_{tool} denote the values of the *Expert Agent* and the best standalone tool, respectively.

Overall, the *Expert Agents* consistently outperformed the best standalone tools on nearly all tasks and metrics. In classification, standard-plane accuracy improved from 0.914 to 0.927 and brain sub-plane κ from 0.830 to 0.856, indicating more robust and consistent plane recognition. In segmentation, abdomen DSC rose from 0.902 to 0.937 while HD95 dropped from 4.20 to 2.32, reflecting substantial gains in both regional overlap and boundary precision. In biometry, the largest improvement appeared in AC measurement (MAE: 9.94 \rightarrow 5.53), with GA estimation MAE also decreasing from 1.32 to 1.23. These results confirm that deterministic multi-tool fusion within *Expert Agents* yields more robust and clinically reliable predictions than any individual best model.

4.8. Ablation Study

To isolate the contribution of each key component, ablation experiments were conducted on three representative tasks (i.e., Task 2, Task 6, and Task 9) spanning measurement, classification, and biometry. Four variants were examined by selectively disabling: (i) w/o the *Arbiter Agent*, defaulting to majority voting among Voters; (ii) w/o the *Expert Agents*, using only one tool; (iii) w/o the DPEA mechanism, collapsing dual-path integration into a single source; and (iv) w/o the Evidence bank, preventing access to consolidated intermediate evidence.

All four components proved indispensable (Tables 6 and 7). Disabling DPEA caused the largest drop (accuracy: 0.8834 \rightarrow 0.7114; report score: 1.1428 \rightarrow 1.0210), confirming that the synergy between deliberative reasoning and computational evidence is the cornerstone of reliable decision-making. Removing *Expert Agents* (accuracy: 0.7649; report: 1.0613) and the *Arbiter Agent* (accuracy: 0.7490; report: 1.0889) further underscored the necessity of tool-grounded evidence and principled evidence arbitration, respectively. Finally, disabling the Evidence bank lowered the report score to 1.0839, indicating that aggregated intermediate evidence materially strengthens factual completeness and coherence.

5. Conclusion

We introduced FetUSAgents and demonstrated its effectiveness as the first tool-augmented multi-agent system for comprehensive fetal ultrasound interpretation in this study. Our findings reveal that FetUSAgents achieves a VQA accuracy of 0.8791 and an macro-F1 score of 0.8721, surpassing the strongest baseline by over 25%, indicating its potential to bridge the gap between isolated task-specific predictors and clinically coherent, evidence-driven reasoning. Furthermore, the proposed Dual-Path Evidence Arbitration mechanism and retrieval-enhanced Evidence bank significantly enhance both decision reliability and report generation quality, effectively reducing hallucination while maintaining factual grounding across diverse clinical tasks. Overall, FetUSAgents offers a scalable framework for reliable fetal ultrasound AI, which can serve as a practical clinical assistant for prenatal imaging and inspire future research on agentic systems in highly specialized medical domains.

References

- Ashkani Chenarlogh, V., Ghelich Oghli, M., Shabanzadeh, A., Sirjani, N., Akhavan, A., Shiri, I., Arabi, H., Sanei Taheri, M., Tarzamni, M.K., 2022. Fast and accurate u-net model for fetal ultrasound image segmentation. *Ultrasound Imaging* 44, 25–38. doi:[10.1177/01617346211069882](https://doi.org/10.1177/01617346211069882).
- Avisdris, N., Jiao, J., Ourselin, S., Vercauteren, T., Bano, S., 2022. Biometrynet: Landmark-based fetal biometry estimation from standard ultrasound planes, in: *Medical Image Computing and Computer Assisted Intervention – MICCAI 2022*, Springer, Cham. doi:[10.1007/978-3-031-16440-8_27](https://doi.org/10.1007/978-3-031-16440-8_27).
- Bai, S., Cai, Y., Chen, R., Chen, K., Chen, X., Cheng, Z., Deng, L., Ding, W., Gao, C., Ge, C., Ge, W., Guo, Z., Huang, Q., Huang, J., Huang, F., et al., 2025. Qwen3-VL technical report. *arXiv e-prints*, arXiv:2511.21631doi:[10.48550/arXiv.2511.21631](https://doi.org/10.48550/arXiv.2511.21631), [arXiv:2511.21631](https://arxiv.org/abs/2511.21631).
- Bano, S., Vasconcelos, F., Amo-Aparicio, J., Teles Rodrigues, P., Curado, I., Dall’Asta, A., David, A.L., Deprest, J., Ourselin, S., Vercauteren, T., Melbourne, A., 2021. Autofb: Automating fetal biometry estimation from standard ultrasound planes, in: *Medical Image Computing and Computer Assisted Intervention – MICCAI 2021*, Springer, Cham. doi:[10.1007/978-3-030-87234-2_22](https://doi.org/10.1007/978-3-030-87234-2_22).
- Baumgartner, C.F., Kamnitsas, K., Matthew, J., Fletcher, T.P., Smith, S., Koch, L.M., Kainz, B., Rueckert, D., 2017. Sononet: Real-time detection and localisation of fetal standard scan planes in freehand ultrasound. *IEEE Transactions on Medical Imaging* 36, 2204–2215. doi:[10.1109/TMI.2017.2712367](https://doi.org/10.1109/TMI.2017.2712367).
- Belciug, S., 2024. Fetal planes and organs. URL: <https://doi.org/10.5281/zenodo.14093338>, doi:[10.5281/zenodo.14093338](https://doi.org/10.5281/zenodo.14093338).
- Burgos-Artizzu, X.P., Coronado-Gutiérrez, D., Valenzuela-Alcaraz, B., Bonet-Carne, E., Eixarch, E., Crispi, F., Gratacós, E., 2020a. Evaluation of deep convolutional neural networks for automatic classification of common maternal fetal ultrasound planes. *Scientific Reports* 10, 10200. doi:[10.1038/s41598-020-67076-5](https://doi.org/10.1038/s41598-020-67076-5).

- Burgos-Artizzu, X.P., Coronado-Gutiérrez, D., Valenzuela-Alcaraz, B., et al., 2020b. Evaluation of deep convolutional neural networks for automatic classification of common maternal fetal ultrasound planes. *Scientific Reports* 10, 10200. doi:[10.1038/s41598-020-67076-5](https://doi.org/10.1038/s41598-020-67076-5).
- ByteDance Seed, 2026. Seed2.0.
- Chen, G., Bai, J., Ou, Z., et al., 2024a. Psfhs: Intrapartum ultrasound image dataset for ai-based segmentation of pubic symphysis and fetal head. *Scientific Data* 11, 436. doi:[10.1038/s41597-024-03266-4](https://doi.org/10.1038/s41597-024-03266-4).
- Chen, J., Gui, C., Ouyang, R., Gao, A., Chen, S., Chen, G.H., Wang, X., Zhang, R., Cai, Z., Ji, K., Yu, G., Wan, X., Wang, B., 2024b. Huatuogpt-vision, towards injecting medical visual knowledge into multimodal llms at scale. [arXiv:2406.19280](https://arxiv.org/abs/2406.19280).
- Chen, Y., Bai, X., Pan, Y., Zhou, Z., Yuille, A., 2026. Meissa: Multi-modal Medical Agentic Intelligence. *arXiv e-prints* , arXiv:2603.09018doi:[10.48550/arXiv.2603.09018](https://doi.org/10.48550/arXiv.2603.09018), [arXiv:2603.09018](https://arxiv.org/abs/2603.09018).
- Da Correggio, K.S., Noya Galluzzo, R., Santos, L.O., et al., 2023. Fetal abdominal structures segmentation dataset using ultrasonic images. doi:[10.17632/4gcpm9dsc3.1](https://doi.org/10.17632/4gcpm9dsc3.1).
- DeepSeek-AI, Liu, A., Mei, A., Lin, B., Xue, B., Wang, B., Xu, B., Wu, B., Zhang, B., Lin, C., Dong, C., Lu, C., Zhao, C., Deng, C., Xu, C., et al., 2025. DeepSeek-V3.2: Pushing the frontier of open large language models. *arXiv e-prints* , arXiv:2512.02556doi:[10.48550/arXiv.2512.02556](https://doi.org/10.48550/arXiv.2512.02556), [arXiv:2512.02556](https://arxiv.org/abs/2512.02556).
- Deng, J., Dong, W., Socher, R., Li, L.J., Li, K., Li, F.F., 2009. ImageNet: A large-scale hierarchical image database, in: 2009 IEEE Conference on Computer Vision and Pattern Recognition, pp. 248–255. doi:[10.1109/CVPR.2009.5206848](https://doi.org/10.1109/CVPR.2009.5206848).
- Dosovitskiy, A., Beyer, L., Kolesnikov, A., Weissenborn, D., Zhai, X., Unterthiner, T., Dehghani, M., Minderer, M., Heigold, G., Gelly, S., Uszkoreit, J., Houlsby, N., 2021. An image is worth 16x16 words: Transformers for image recognition at scale, in: International Conference on Learning Representations.

- Fiorentino, M.C., Villani, F.P., Di Cosmo, M., Frontoni, E., Moccia, S., 2023a. A review on deep-learning algorithms for fetal ultrasound-image analysis. *Medical Image Analysis* 83, 102629. doi:[10.1016/j.media.2022.102629](https://doi.org/10.1016/j.media.2022.102629).
- Fiorentino, M.C., Villani, F.P., Di Cosmo, M., Frontoni, E., Moccia, S., 2023b. A review on deep-learning algorithms for fetal ultrasound-image analysis. *Medical Image Analysis* 83, 102629. doi:[10.1016/j.media.2022.102629](https://doi.org/10.1016/j.media.2022.102629).
- González, D., Barrientos, J.P., Perez, M., Fajardo, J., Reyna, F., Lara, A., 2024. Natalia: Pbf-us1 (phantom blind-sweeps for fetal ultrasound scanning). doi:[10.5281/zenodo.14193949](https://doi.org/10.5281/zenodo.14193949).
- Google, 2025. Gemini 3 pro preview.
- Google DeepMind, 2025. Gemini 3 flash.
- Grembowski, D., Schaefer, J., Johnson, K.E., Fischer, H., Moore, S.L., Tai-Seale, M., Ricciardi, R., Fraser, J.R., Miller, D., LeRoy, L., AHRQ MCC Research Network, 2014. A conceptual model of the role of complexity in the care of patients with multiple chronic conditions. *Medical Care* 52, S7–S14. doi:[10.1097/MLR.000000000000045](https://doi.org/10.1097/MLR.000000000000045).
- He, D., Wang, H., Yaqub, M., 2025. Advancing Fetal Ultrasound Image Quality Assessment in Low-Resource Settings. *arXiv e-prints*, arXiv:2507.22802doi:[10.48550/arXiv.2507.22802](https://doi.org/10.48550/arXiv.2507.22802), [arXiv:2507.22802](https://arxiv.org/abs/2507.22802).
- He, F., Wang, Y., Xiu, Y., Zhang, Y., Chen, L., 2021. Artificial intelligence in prenatal ultrasound diagnosis. *Frontiers in Medicine* 8, 729978. doi:[10.3389/fmed.2021.729978](https://doi.org/10.3389/fmed.2021.729978).
- van den Heuvel, T.L.A., de Bruijn, D., de Korte, C.L., Ginneken, B.v., 2018. Automated measurement of fetal head circumference using 2d ultrasound images. *PLOS ONE* 13, 1–20. doi:[10.1371/journal.pone.0200412](https://doi.org/10.1371/journal.pone.0200412).
- Hu, E.J., yelong shen, Wallis, P., Allen-Zhu, Z., Li, Y., Wang, S., Wang, L., Chen, W., 2022. LoRA: Low-rank adaptation of large language models, in: *International Conference on Learning Representations*.
- Isensee, F., Jaeger, P.F., Kohl, S.A.A., Petersen, J., Maier-Hein, K.H., 2021. nnu-net: a self-configuring method for deep learning-based biomedical image segmentation. *Nature Methods* 18, 203–211. doi:[10.1038/s41592-020-01008-z](https://doi.org/10.1038/s41592-020-01008-z).

- Jiang, S., Wang, Y., Song, S., Hu, T., Zhou, C.e.a., 2025. Hulu-Med: A Transparent Generalist Model towards Holistic Medical Vision-Language Understanding. arXiv e-prints , arXiv:2510.08668doi:[10.48550/arXiv.2510.08668](https://doi.org/10.48550/arXiv.2510.08668), [arXiv:2510.08668](https://arxiv.org/abs/2510.08668).
- Jiao, J., Zhou, J., Li, X., Xia, M., Huang, Y., Huang, L., Wang, N., Zhang, X., Zhou, S., Wang, Y., Guo, Y., 2024. Usfm: A universal ultrasound foundation model generalized to tasks and organs towards label efficient image analysis. *Medical Image Analysis* 96, 103202. doi:[10.1016/j.media.2024.103202](https://doi.org/10.1016/j.media.2024.103202).
- Kim, Y., Park, C., Jeong, H., Chan, Y.S., Xu, X., McDuff, D., Lee, H., Ghassemi, M., Breazeal, C., Park, H.W., 2024. MDAgents: An adaptive collaboration of LLMs for medical decision-making, in: *The Thirty-eighth Annual Conference on Neural Information Processing Systems*.
- Kiserud, T., Piaggio, G., Carroli, G., Widmer, M., Carvalho, J., et al., 2017. The world health organization fetal growth charts: A multinational longitudinal study of ultrasound biometric measurements and estimated fetal weight. *PLOS Medicine* 14, 1–36. doi:[10.1371/journal.pmed.1002220](https://doi.org/10.1371/journal.pmed.1002220).
- Krishna, T.B., Kokil, P., 2023. Automated classification of common maternal fetal ultrasound planes using multi-layer perceptron with deep feature integration. *Biomedical Signal Processing and Control* 86, 105283. doi:<https://doi.org/10.1016/j.bspc.2023.105283>.
- Krishna, T.B., Kokil, P., 2024. Standard fetal ultrasound plane classification based on stacked ensemble of deep learning models. *Expert Syst. Appl.* 238. doi:[10.1016/j.eswa.2023.122153](https://doi.org/10.1016/j.eswa.2023.122153).
- LangChain, 2026. Openaiembeddings. LangChain Python API Reference. Accessed: 2026-05-20.
- Li, C., Wong, C., Zhang, S., Usuyama, N., Liu, H., Yang, J., Naumann, T., Poon, H., Gao, J., 2023. LLaVA-med: Training a large language-and-vision assistant for biomedicine in one day, in: *Thirty-seventh Conference on Neural Information Processing Systems Datasets and Benchmarks Track*.
- Lin, X., Xiang, Y., Yu, L., Yan, Z., 2024. Beyond Adapting SAM: Towards End-to-End Ultrasound Image Segmentation via Auto Prompting , in: *proceedings of Medical Image Computing and Computer Assisted Intervention – MICCAI 2024*, Springer Nature Switzerland.

- Liu, S., Bao, L., Yang, Q., Geng, W., Zheng, B., Li, C., Chen, W., Peng, H., Yuan, Y., 2026. MedSAM-Agent: Empowering Interactive Medical Image Segmentation with Multi-turn Agentic Reinforcement Learning. arXiv e-prints , arXiv:2602.03320doi:[10.48550/arXiv.2602.03320](https://doi.org/10.48550/arXiv.2602.03320), [arXiv:2602.03320](https://arxiv.org/abs/2602.03320).
- Liu, Z., Mao, H., Wu, C.Y., Feichtenhofer, C., Darrell, T., Xie, S., 2022. A convnet for the 2020s, in: Proceedings of the IEEE/CVF Conference on Computer Vision and Pattern Recognition (CVPR), pp. 11976–11986.
- Lu, Y., Zhou, M., Zhi, D., Zhou, M., Jiang, X., Qiu, R., Ou, Z., Wang, H., Qiu, D., Zhong, M., Lu, X., Chen, G., Bai, J., 2022. The jnu-ifm dataset for segmenting pubic symphysis-fetal head. Data in Brief 41, 107904. doi:<https://doi.org/10.1016/j.dib.2022.107904>.
- Lyu, X., Liang, Y., Chen, W., Ding, M., Yang, J., Huang, G., Zhang, D., He, X., Shen, L., 2025. WSI-Agents: A Collaborative Multi-Agent System for Multi-Modal Whole Slide Image Analysis , in: proceedings of Medical Image Computing and Computer Assisted Intervention – MICCAI 2025, Springer Nature Switzerland.
- Maani, F., Saeed, N., Saleem, T., Farooq, Z., Alasmawi, H., Diehl, W., Mohammad, A., Waring, G., Valappi, S., Bricker, L., Yaqub, M., 2025. FetalCLIP: A Visual-Language Foundation Model for Fetal Ultrasound Image Analysis. doi:[10.48550/arXiv.2502.14807](https://doi.org/10.48550/arXiv.2502.14807), [arXiv:2502.14807](https://arxiv.org/abs/2502.14807).
- Mao, Y., Xu, W., Qin, Y., et al., 2026. CT-Agent: A multimodal-llm agent for 3d ct radiology question answering. Science China Information Sciences 69, 150107. doi:[10.1007/s11432-025-4818-7](https://doi.org/10.1007/s11432-025-4818-7).
- Mei, X., Liu, Z., Robson, P.M., Marinelli, B., Huang, M., Doshi, A., Jacobi, A., Cao, C., Link, K.E., Yang, T., Wang, Y., Greenspan, H., Deyer, T., Fayad, Z.A., Yang, Y., 2022. Radimagenet: An open radiologic deep learning research dataset for effective transfer learning. Radiology: Artificial Intelligence 4, e210315. doi:[10.1148/ryai.210315](https://doi.org/10.1148/ryai.210315). PMID: 36204533.
- Mikołaj, K.W., Christensen, A.N., Taksøe-Vester, C.A., et al., 2025. Predicting abnormal fetal growth using deep learning. npj Digital Medicine 8, 318. doi:[10.1038/s41746-025-01704-0](https://doi.org/10.1038/s41746-025-01704-0).

- Olagunju, O.J., Egbo, B., Osanyinlusi, O.O., Olagunju, O.E., Olorunmolu, S.E., 2025. Assessing the role of ultrasound scanning in improving pregnancy outcomes in potiskum and neighboring rural communities in yobe state, nigeria. *Cureus* 17, e79768. doi:[10.7759/cureus.79768](https://doi.org/10.7759/cureus.79768).
- OpenAI, 2025. Gpt-5.1: A smarter, more conversational chatgpt.
- OpenAI, 2026a. Introducing gpt-5.4.
- OpenAI, 2026b. text-embedding-3-small model. OpenAI API model documentation. Accessed: 2026-05-20.
- Pham, H.H., Quoc Khanh, L.T., Nguyen, H.T., Vi Vu, N.L., Dinh, Q.V., Nguyen, T.H., Li, X., Xu, M., 2025. Fetal-bcp: Addressing empirical distribution gap in semi-supervised fetal ultrasound segmentation, in: 2025 IEEE 22nd International Symposium on Biomedical Imaging (ISBI), pp. 1–4. doi:[10.1109/ISBI60581.2025.10980925](https://doi.org/10.1109/ISBI60581.2025.10980925).
- Pu, B., Lu, Y., Chen, J., Li, S., Zhu, N., Wei, W., Li, K., 2022. Mobileunet-fpn: A semantic segmentation model for fetal ultrasound four-chamber segmentation in edge computing environments. *IEEE Journal of Biomedical and Health Informatics* 26, 5540–5550. doi:[10.1109/JBHI.2022.3182722](https://doi.org/10.1109/JBHI.2022.3182722).
- Qi, T., Bu, S., Xiang, Y., Dai, Z., 2026. EviAgent: Evidence-Driven Agent for Radiology Report Generation. arXiv e-prints , arXiv:2603.13956doi:[10.48550/arXiv.2603.13956](https://doi.org/10.48550/arXiv.2603.13956), [arXiv:2603.13956](https://arxiv.org/abs/2603.13956).
- Qwen Team, 2025. Qwen3-max: Just scale it.
- Salomon, L.J., Alfirevic, Z., Berghella, V., Bilardo, C., Hernandez-Andrade, E., Johnsen, S.L., Kalache, K., Leung, K.Y., Malinger, G., Munoz, H., Prefumo, F., Toi, A., Lee, W., ISUOG Clinical Standards Committee, 2011. Practice guidelines for performance of the routine mid-trimester fetal ultrasound scan. *Ultrasound in Obstetrics & Gynecology* 37, 116–126. doi:[10.1002/uog.8831](https://doi.org/10.1002/uog.8831).
- Sappia, M.S., de Korte, C.L., van Ginneken, B., Ninalga, D., Kondo, S., et al., 2025. Acouslic-ai challenge report: Fetal abdominal circumference measurement on blind-sweep ultrasound data from low-income countries. *Medical Image Analysis* 105, 103640. doi:[10.1016/j.media.2025.103640](https://doi.org/10.1016/j.media.2025.103640).

- Sellergren, A., Kazemzadeh, S., Jaroensri, T., Kiraly, A., Traverse, M., et al., 2025. Medgemma technical report. arXiv e-prints , arXiv:2507.05201doi:[10.48550/arXiv.2507.05201](https://doi.org/10.48550/arXiv.2507.05201), [arXiv:2507.05201](https://arxiv.org/abs/2507.05201).
- Sendra-Balcells, C., Campello, V.M., Torrents-Barrena, J., et al., 2023. Generalisability of fetal ultrasound deep learning models to low-resource imaging settings in five african countries. *Scientific Reports* 13, 2728. doi:[10.1038/s41598-023-29490-3](https://doi.org/10.1038/s41598-023-29490-3).
- Shu, X., Chang, F., Zhang, X., Shao, C., Yang, X., 2022. Ecau-net: Efficient channel attention u-net for fetal ultrasound cerebellum segmentation. *Biomedical Signal Processing and Control* 75, 103528. doi:<https://doi.org/10.1016/j.bspc.2022.103528>.
- Sippel, S., Muruganandan, K., Levine, A., Shah, S., 2011. Review article: Use of ultrasound in the developing world. *International Journal of Emergency Medicine* 4, 72. doi:[10.1186/1865-1380-4-72](https://doi.org/10.1186/1865-1380-4-72).
- Tang, X., Zou, A., Zhang, Z., Li, Z., Zhao, Y., Zhang, X., Cohan, A., Gerstein, M., 2024. MedAgents: Large language models as collaborators for zero-shot medical reasoning, in: *Findings of the Association for Computational Linguistics: ACL 2024*, Association for Computational Linguistics, Bangkok, Thailand. pp. 599–621. doi:[10.18653/v1/2024.findings-acl.33](https://doi.org/10.18653/v1/2024.findings-acl.33).
- Venturini, L., Budd, S., Farruggia, A., et al., 2025. Whole examination ai estimation of fetal biometrics from 20-week ultrasound scans. *npj Digital Medicine* 8, 22. doi:[10.1038/s41746-024-01406-z](https://doi.org/10.1038/s41746-024-01406-z).
- Wang, F., Silvestre, G., Curran, K.M., 2024. Segmenting Fetal Head with Efficient Fine-tuning Strategies in Low-resource Settings: an empirical study with U-Net. arXiv e-prints , arXiv:2407.20086doi:[10.48550/arXiv.2407.20086](https://doi.org/10.48550/arXiv.2407.20086), [arXiv:2407.20086](https://arxiv.org/abs/2407.20086).
- Wang, F., Whelan, K., Silvestre, G., Curran, K.M., 2024. Generative diffusion model bootstraps zero-shot classification of fetal ultrasound images in underrepresented african populations, in: *Perinatal, Preterm and Paediatric Image Analysis*, Springer, Cham. pp. 143–154. doi:[10.1007/978-3-031-73260-7_13](https://doi.org/10.1007/978-3-031-73260-7_13).
- Wang, Z., Cai, L., Low, C.H., Liu, H., Wu, J., Wang, J., Wang, R., Song, L., Bian, J., Fu, J., Jin, Y., 2026. 3DMedAgent: Unified

- Perception-to-Understanding for 3D Medical Analysis. arXiv e-prints , arXiv:2602.18064doi:[10.48550/arXiv.2602.18064](https://doi.org/10.48550/arXiv.2602.18064), [arXiv:2602.18064](https://arxiv.org/abs/2602.18064).
- Wu, Q., Bansal, G., Zhang, J., Wu, Y., Li, B., Zhu, E., Jiang, L., Zhang, X., Zhang, S., Liu, J., Awadallah, A.H., White, R.W., Burger, D., Wang, C., 2024. Autogen: Enabling next-gen LLM applications via multi-agent conversations, in: First Conference on Language Modeling.
- Xiao, T., Liu, Y., Zhou, B., Jiang, Y., Sun, J., 2018. Unified perceptual parsing for scene understanding, in: Proceedings of the European Conference on Computer Vision (ECCV).
- Yan, L., Li, Q., Fu, K., Zhou, X., Zhang, K., 2025. Progress in the application of artificial intelligence in ultrasound-assisted medical diagnosis. *Bioengineering* 12, 288. doi:[10.3390/bioengineering12030288](https://doi.org/10.3390/bioengineering12030288).
- Zakka, C., Shad, R., Chaurasia, A., Dalal, A.R., Kim, J.L.e.a., 2024. Almanac - retrieval-augmented language models for clinical medicine. *NEJM AI* 1. doi:[10.1056/aioa2300068](https://doi.org/10.1056/aioa2300068). epub 2024 Jan 25. PMID: 38343631; PMCID: PMC10857783.
- Zeng, W., Luo, J., Cheng, J., Lu, Y., 2022. Efficient fetal ultrasound image segmentation for automatic head circumference measurement using a lightweight deep convolutional neural network. *Medical Physics* 49, 5081–5092. doi:[10.1002/mp.15700](https://doi.org/10.1002/mp.15700). epub 2022 May 24. PMID: 35536111.
- Zhou, S., Yu, K., Wang, S., Xie, W., Zhan, Z., Tsai, M.H., Chung, Y.H., Hou, S., Zhou, H., Zeng, M., Ramu, B., Chen, L.Y., Xie, F., Zhang, R., 2026. HeartAgent: An Autonomous Agent System for Explainable Differential Diagnosis in Cardiology. arXiv e-prints , arXiv:2603.10764doi:[10.48550/arXiv.2603.10764](https://doi.org/10.48550/arXiv.2603.10764), [arXiv:2603.10764](https://arxiv.org/abs/2603.10764).
- Zhou, Z., Lu, Y., Bai, J., Campello, V.M., Feng, F., Lekadir, K., 2025. Segment anything model for fetal head-pubic symphysis segmentation in intrapartum ultrasound image analysis. *Expert Systems with Applications* 263, 125699. doi:<https://doi.org/10.1016/j.eswa.2024.125699>.